Heliyon 8 (2022) e11620

Contents lists available at ScienceDirect

Heliyon

journal homepage: www.cell.com/heliyon

Review article

PVDF composite nanofibers applications

Sedigheh Aghayari *

Sharif University of Technology, Tehran, Iran

ARTICLE INFO

Keywords:
PVDF
Electrospinning
Nanofibers
Composites

ABSTRACT

Polyvinylidene fluoride (PVDF) has special piezo/pyro/ferroelectric, flexibility, low weight, biocompatibility, economical, good chemical/thermal, and high mechanical properties, such as excellent nontoxic fiber/film formation. It has polar and nonpolar phases of α, β, γ, ε, and δ, in which the nonpolar α phase is the most stable one. However, the β phase is the best because it has good piezo/pyro/ferroelectric properties. Copolymers are attractive due to their low weight, nontoxic, chemical acid resistance, flexibility, and ease of processing. These aspects result in their applications in many fields. They are used for piezoelectric nanogenerators, cooling/heating sensors, electronic devices (fuel cells, lithium-ion batteries (as separators), dye-sensitive solar cells), filtration, oil/water separation, and photoelectric nanodevices. This review highlights the main aspects of the last decade's studies and focuses on the synthesis methods of PVDF nanofibers and their properties, leading to their applications in different sectors of industry.

1. Introduction

Due to the excellent properties of PVDF, nanostructures have applications in smart wound dressings, smart machine seats, self-cleaning filters, cooling and heating sensors [1], electronic devices, ultrafiltration, heavy metal removal, photocatalysts, desalinated water osmosis, oil/water separation [2], and photoelectric devices [3].

Electrospun nanowebs have a high specific surface area, adjustable porosity, interconnective pores, microscale interstitial distance, and flexibility because of their different sizes and morphologies. Due to these advantages, they are attractive in tissue engineering, sensors, wearable electronics, and water purification [4]. However, other methods, such as centrifugal spinning [5] and blow spinning [6], have recently gained significant attraction. Because of the limitations of electrospinning, including high voltage sources, it requires toxic organic solvents and low production rates in most cases [5]. Depending on the synthesis conditions, nanofibers can have different morphologies, such as mesoporous fibers [7]. These morphologies result in a higher specific surface area of nanofibers that can enhance their properties, especially sensing operation.

The PVDF nanofibers with nanostructures give hydrophobic, controllable structural properties (length-to-diameter ratio, high surface-to-weight ratio, and small diameter (tens to hundreds of nanometers)) and piezo/pyro/ferroelectric properties (easy to control by adjusting production parameters) makes them more exposed to attention.

This review focuses on the synthesis methods, properties, and applications of PVDF nanofibers.

2. PVDF nanofiber

The following is focused on PVDF nanofiber synthesis methods, their main properties and applications in other industries. Many methods have been developed to produce nanofibers, including centrifugal spinning [5], blow spinning [6], and electrospinning [8]. Most studies in the last decade have focused on electrospinning with polymer solutions, but other methods have been developed recently because of some limitations. Forcespinning is centrifugal spinning that uses centrifugal forces instead of high voltage to thin a *jet* flow [5]. Two parallel concentric fluid flows, including polymer solution flow and compact airflow surrounding the polymer solution, exist in blow spinning. The jet flow is produced and thinned with airflow and evaporates solvent fibers in the same direction as the gas flow deposit. This method does not have a high voltage despite electrospinning [5]. Compared to the solution, electrospinning with melt is more economical and environmentally friendly because of the absence of organic solvents and ease of processing [8].

Investigating and utilizing PVDF nanofibers with different nanoparticles has recently gained great attention. Better and multifunctional properties result from using other structures, such as small molecules, polymers, and nanostructures. The morphology of nanofibers can change with controlling production parameters, and it has a vital role in increasing the material properties. For example, nanofiber morphology is useful in piezo/pyro/ferroelectric properties because the reduction in diameter can increase the β phase due to more thinning [9]. It has been shown that the increased specific surface area can benefit gas absorption

* Corresponding author.
E-mail address: 1415he@gmail.com.

https://doi.org/10.1016/j.heliyon.2022.e11620
Received 21 May 2022; Received in revised form 7 August 2022; Accepted 9 November 2022

[7]. Different metal and metal oxide elements as dopants, such as Ce and MoS2, are used to raise the PVDF properties. Moreover, knowledge and utilization of the piezo/pyro/ferroelectric properties, hydrophobicity, and chemical and mechanical stability of nanostructures can enable the development of sensors, nano/photoelectric devices, and other exciting applications. Therefore, some details based on the piezo/pyro/ferroelectric properties, hydrophobicity, and chemical and mechanical stability of recently developed PVDF nanofibers in various applications are discussed in the following.

2.1. Piezoelectric properties

The ceramic nanofibers with high piezoelectric properties do not have enough flexibility and wearing ability, demanding using piezoelectric polymers as a solution. Among choices, PVDF has the most piezoelectric properties, yet not higher than ceramics. There are many methods for generating the β phase, including mechanical drawing, thermal annealing, or electrical polling. However, all of them have limitations for PVDF. In this regard, methods to improve the piezoelectric properties of PVDF include electrospinning and doping, which are the focus point in [10].

In electrospinning, dipoles are parallel to the layer thickness, causing the layer polarization.

Investigating the β phase content is practical to determine the piezoelectric properties of PVDF. In this study, Fourier-transform infrared spectroscopy (FTIR), X-ray diffraction (XRD), piezoresponse force microscopy (PFM), field emission scanning electron microscopy (FESEM), and differential scanning calorimetry (DSC) can be helpful.

Utilizing pressure stresses results in layer polarization because of changing the total momentum of the dipole and thickness of the layer under pressure. Consequently, charges produce and flow from the external circuit. After removing these external stresses, the polarization saves, and current flows in the opposite direction, making the inverse signal. Therefore, the output is the usual AC signal (Figure 1) [9].

Furthermore, FESEM is used to investigate the morphology of nanofibers from which the diameter of the nanofibers can be extracted. Figure 2 and Table 1 show the results reported by different researchers. Furthermore, FESEM is used to investigate the morphology of nanofibers, from which the diameter of the nanofibers can be extracted. Figure 2 and Table 1 show the results reported by different researchers. According to the doping results, the conductivity of the solution increased. So, the diameter of the nanofibers decreased, and the piezoelectric property increased. On the other hand, by increasing the solution viscosity, the diameter of the nanofiber increases in Sample 2. Moreover, cerium ions were added in Sample 3 and graphene, which helped reduce the diameter.

Moreover, FTIR is a suitable choice to define the exact β phase content and investigate crystallinity. Table 2 displays the result analysis. Among different wavelengths for all phases, bands at 840 are used for the β phase and 833 for the gamma phase. Since other bands are not very strong, they cannot be considered in the analysis [16]. Also, Figure 3 and Table 3 demonstrate the results of other works. It is clear that the peaks for the β phase increase after doping and decrease for others. Therefore, FTIR can show encasement of the β phase. Indeed, there is a formula for determining the content of each phase by calculating the baseline-corrected absorbance and wavenumbers. However, we can see whether the phases became stronger or not by looking at the curves (see Figure 3).

According to the doping results, the β phase increases, leading to higher piezoelectric properties. In other words, this test makes investigation of the crystallinity possible. These are the analysis results of this test (for Kα1 = 1.5405600 Å) according to Table 4. Also, Figure 4 presents the peaks of different phases, and each peak belongs to an individual crystal plane [16]. The findings of the researchers' works were summarized in Table 5. By paying attention to peaks, it is possible to understand whether the process was successful in increasing the individual phase. The stronger the peaks of each phase becomes, the more the phase increases. Moreover, from Table 5, it is visible that adding any dopants results in a higher β phase content, indicating that all dopants can lead to a higher β phase content. Consequently, XRD can be used to recognize whether the β phase raises.

According to the results from using additives, the piezoelectric property increases. PFM is a simple method that uses the contact mode to evaluate the single fiber piezoelectric constant. The effective piezoelectric constant $d_{33,\ eff}$ is obtained from the following equation:

where A, V, and ε are the amplitude, AC voltage, and correction factor, respectively, which are illustrated by alternative electrical polling of a standard lithium niobate. Also, high $d_{33,eff}$ indicates high piezoelectric properties [10]. It can be seen that when the effective piezoelectric constant increases, the piezoelectric properties become stronger. In Table 5, all dopants result in a higher effective piezoelectric constant, which can be confirmed by PFM. For this section, an electrospun layer with the electrode(s) is used, and by applying pressure, such as human hand force, the pressure is converted into electricity. As a result, it is possible to measure the electrical voltage.

As seen in Table 5, the piezoelectric output increased by doping, and the effect is entirely adaptive to the results of previous tests.

It was concluded that FESEM, SEM, FTIR, XRD, and PFM analysis or measuring the voltage and current outputs of piezoelectric tests help determine whether the piezoelectric property increases. Doping is a suitable way to improve the piezoelectric effect and oil separation efficiency of electrospun PVDF webs. Furthermore, there are other methods to improve piezoelectric output. For instance, there are also other

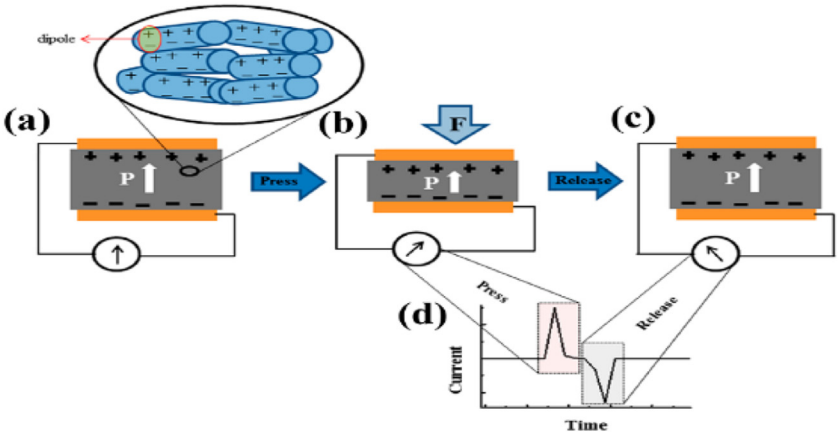

Figure 1. Nanogenerator working mechanism at (a) the initial state (enlarged view shows that the dipoles are parallel to the thickness direction), (b) the pressed state, and (c) the released state. (d) Press and release states result in positive and negative peaks of AC generated from nanogenerator [9].

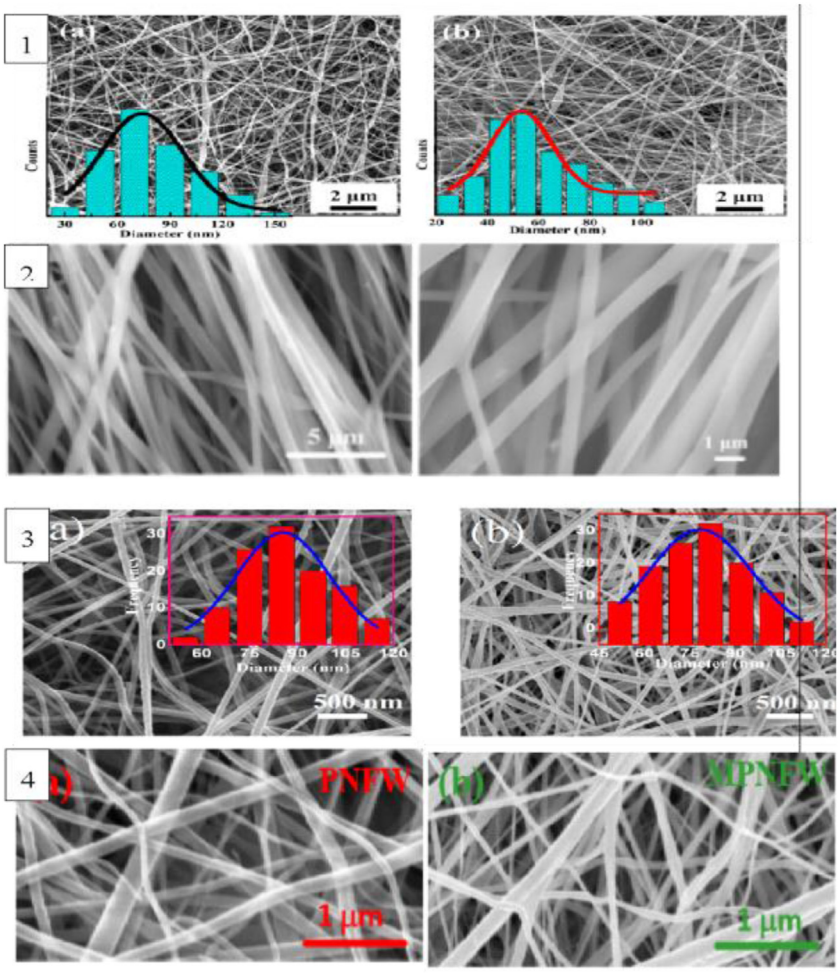

Figure 2. FESEM images of nanofibers with/without dopants: 1) TiO_2 [9], 2) BTO [10], 3) G [11], and 4) MoS_2 [12].

Table 1. Diameters of nanofibers with/without dopants. Column 4 shows the diameter of PVDF nanofibers without dopants, and column 2 shows the diameter of PVDF nanofibers with dopants.

Sample	Diameter (nm)	Sample	Diameter (nm)	Diameter changes (%)	Source
PVDF/TiO_2	-	PVDF	-	decreased	[9]
P(VDF–TrFE)/ BTO	-	PVDF	400	-	[10]
PVDF/Ce^{3+}/G	80	PVDF	85	-6	[11]
PVDF/MoS_2	75 ± 10	PVDF	107 ± 5	-30	[12]
PPy/PVDF	325 ± 143	PVDF	453 ± 153	-28	[13]
PANI/PVDF	390 ± 138	PVDF	453 ± 153	-14	[13]
P-LGA/PVDF	2512 ± 1182	PVDF	453 ± 153	454	[13]
PVDF-ILS4	592 ± 404	PVDF	321 ± 152	84	[1]
PVDF/Ag	169 ± 21	PVDF	156 ± 13	8	[14]
PVDF/ZnO	195	PVDF	240	-19	[15]

methods for improving piezoelectric output, such as increasing specific surface area, for example, by mesoporous nanofibers [18], penetrated electrodes [10], and plasma treatment [19]. Also, benefiting the test and layer conditions [20] (layer thickness, polymer type, the nanofiber diameter, nanofiber alignment in web, layer surface area, and finding the conditions that make higher output), and the electrode (electrode type [21] and type of method of applying the electrode on the layer [22]), which is a subject of the next paper.

Table 2. Wavelengths of picks of different phases of PVDF [16].

Wavenumber (cm^{-1})		
α	β	γ
408	510	431
532	840	512
614	1279	776
766		812
795		833
855		840
976		1234

2.2. Ferroelectric property

In contrast with different nanoparticles, such as TiO_2, $SrTiO_3$, and $BaTiO_3$, ferrite nanoparticles have superior efficiency in increasing the electroactive phase of PVDF and its copolymers. These nanoparticles can increase the magnetic, ferroelectric, and dielectric properties of PVDF. Moreover, $NiFe_2O_4$ is an essential ferrite material that has applications in MRI contrast agents and media with the capability of saving high magnetic density, ferrofluid, color imaging, catalysts, and microwave devices. High information-saving efficiency, nanomagnetic properties, and ferroelectric properties result in good energy production from the piezoelectric property when they cooperate in PVDF [23].

Adding nanoparticles, especially ferrite nickel, results in the nucleation of the ferroelectric phase combined with phase conversion due to

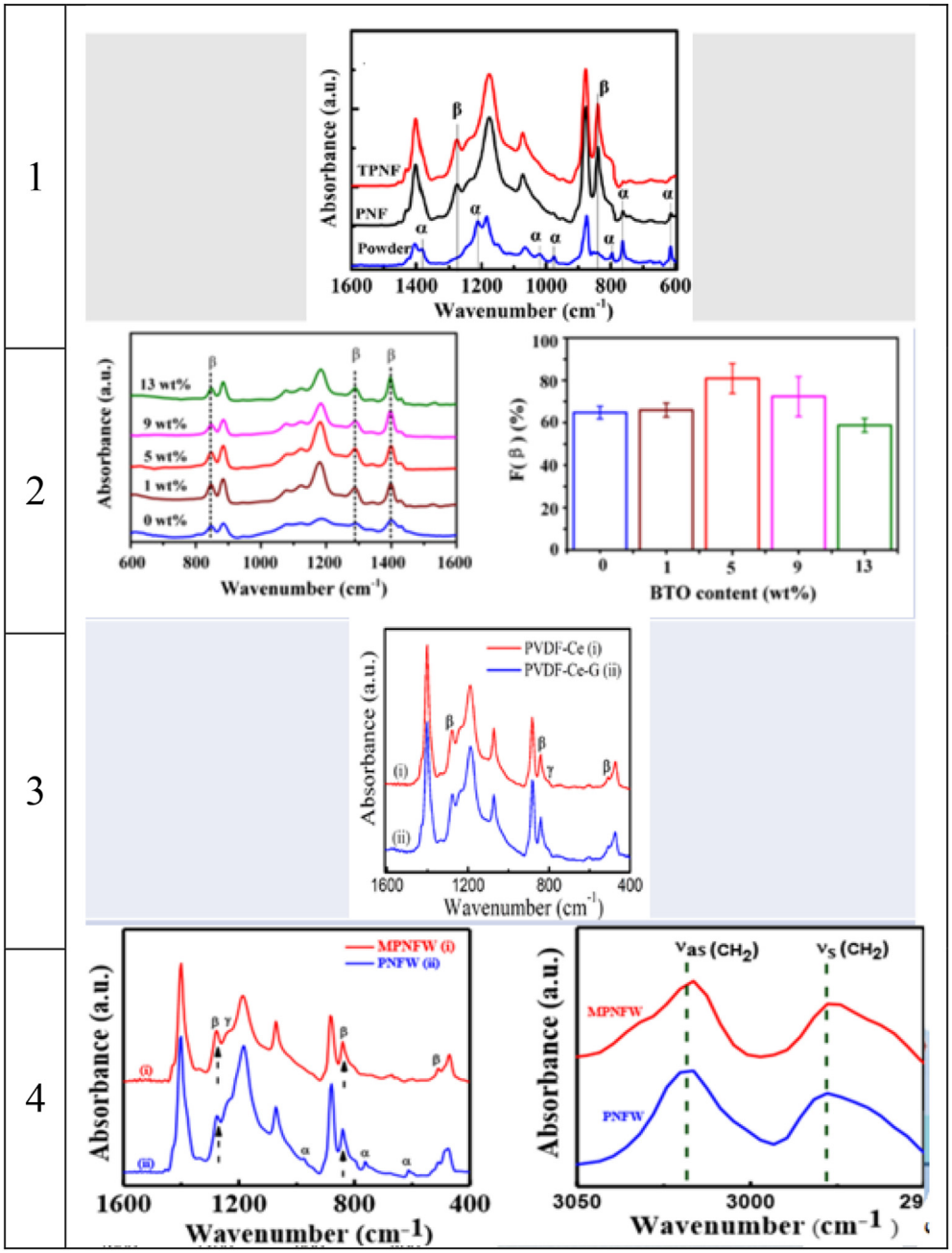

Figure 3. FTIR images of nanofibers with/without: 1) TiO_2 [9], 2) BTO [10], 3) G [11], and 4) MoS_2 [12].

incorporating nanoparticles and increasing crystallinity. However, trapped particles in the amorphous polymer phase result in spherulite growth [23].

By designing a system shown in Figure 5, the ferroelectric properties of all the samples were tested. A frequency generator was applied to provide a range of vibrations (15–45 Hz), and an amplifier was attached to the vibration shaker to amplify the vibrations and transfer them. On the top of the shaker, there is a sample with conductive wires on both sides with a weight of 2.5. According to the vibration frequency, the shaker shakes, and the weight contributes to the pressure force of the sample. These forces show the electrical voltage by changing the dipole moment, and the data-receiving system records these results. Using a resistant box attached to the sample makes it possible to produce voltage to be maximized before recording [23].

The maximum dielectric constant of nanocomposites with 1wt% $NiFe_2O_4$ was 118 in 1 Hz, 24 times higher than that of nanofibers. By adding 2wt%, the additive output voltage was 4 V [23]. The magnetoelectric devices have magnetic sensors, multistate memories, electric field-controlled ferromagnetic resonance devices, and actuators. It is because of the dielectric polarization property obtained by applying a magnetic field and/or inducing magnetization with an external field [23]. To determine the magnetoelectric properties of, PFM was used by applying the magnetic field to determine the piezoelectric and magnetoelectric properties of PVDF/PMMA-Fe_3O_4 nanofibers. The diameter increased by adding nanoparticles. The amplitude compared to iron oxide nanoparticles was much narrower. It signifies a magnetic field effect on the piezoelectric response and magnetoelectric effect to deliver the appropriate electrical signal for nerve and tissue cells biomedically [24].

In addition, $Co0.5Ni0.5Fe_2O_4$/PVDF nanofibers have a higher β phase due to doping compared to PVDF nanofibers influenced by the ferroelectric properties of the layer. The vibrating sample magnetometer

Table 3. β phase contents of nanofibers with/without dopants. Column 4 shows the β phase content of PVDF nanofibers without dopants, and column 2 shows the β phase content of PVDF nanofibers with dopants.

Sample	β phase (%)	Sample	β phase (%)	β phase change (%)	Source
PVDF/TIO2	-	PVDF	-	16	[1]
P(VDF–TrFE)/BTO	81	PVDF	65	16	[11]
PVDF/Ce3+/G	99	PVDF	96	3	[12]
PVDF/MoS2	95	PVDF	92	3	[13]
PPy/PVDF	83.5	PVDF	77.4	6.1	[14]
PANI/PVDF	83.6	PVDF	77.4	6.2	[14]
P-LGA/PVDF	85.3	PVDF	77.4	7.9	[14]
PVDF-ILS4	98.62	PVDF	76.04	22.58	[2]
PVDF/Ag	94	PVDF	83	11	[15]
PVDF/ZnO	92	PVDF	86	6	[16]
PVDF/Pt	99.9	PVDF	76	23.9	[17]

(VSM) method was used to determine ferroelectric properties (Figure 6). The stability of the magnetization of nanoparticles increased owing to the polymer's nonmagnetic nature. So, the resulting web is helpful for water purification, spintronic devices, and magnetic sensors [25]. The ferroelectric properties are also present in tetragonal barium titanate [26] and gold [27] nanoparticles.

Dopamine-functionalized $BaTiO_3$/$BaTiZrO_3$/$BaZrO_3$-PVDF nanofibers have a higher β phase content and better dielectric, ferroelectric (Figure 7), and mechanical properties due to doping. They are appropriate for storing media in electrical devices such as memories with random access ability [28].

2.3. Pyroelectric property

Due to PVDF properties, it is applicable in tactile sensors, energy harvesters, and IR imaging. The PVDF has poor absorption in the visible region and near-infrared, which avoids the effective conversion of light to heat and an electrical signal. The gold nanocages in nanofibers were used to overcome this problem. Combining this method with electrospinning led to a higher β phase content and better piezo/pyroelectric properties. The nanocages can give nanofibers the ability to convert light into heat and, consequently, electricity. Thus, they are suitable for sensing light. By applying tactile force and IR radiation, the output voltage increased 12.6 times (7.2 V), so a piezo/pyroelectric hybrid sensor was constructed [29].

Furthermore, plasmonic nanomaterials for applications from photonic to medical have been developed due to localized surface plasmon resonance (LSPR) and corresponding properties. An example is gold-based nanostructures with a wide range of shapes of non-spherical or complicated structures to produce adjustable LSPR peaks in visible and near-infrared regions. Of them, gold nanocages with hollow spaces and porous walls are very attractive because their LSR usually makes them absorb rather than scatter. The absorption peak is adjustable precisely in the 400–1200 nm region by controlling the wall thickness. These nanocages with strong absorption are efficient photothermal converters for converting a photon to phonon or heat [29]. Additionally, a strong electrostatic interaction between nanoparticles with a positive charge and negative charge of the F atoms in the polymer chain can cause interfacial polarization in the crystalline phase named β [29]. Moreover, gold nanoparticles help change the piezo/pyro/ferroelectric properties of PVDF [23].

2.4. Wettability properties

In lithium-ion batteries (as separators), in addition to high porosity, an excellent intrinsic desire between the separator and electrolyte is necessary for electrochemical operation because the good wetting ability can help faster lithium-ion transfer. Figure 8 displays the wetting ability of the webs by scattering 10 μL of the liquid electrolyte. Although the wetting of the commercial sample was limited, others wetted thoroughly in 2 s. The contact angles of the PE, PVDF, Al_2O_3/SiO_2/PVDF, Al_2O_3/PVDF, and SiO_2/PVDF samples were 25.1°, 18.3, 18.3, 16, and 46.3°, respectively (Figure 9) [8].

It can be due to the polar bands (C–F) in PVDF that prepare strong interactions with polar electrolytes. In contrast, the PE web, prepared from hydrophobic polyolefin, resulted in low wetting with polar liquid electrolyte [8]. The PVDF-HFP nanofibers have hydrophobic webs due to the intrinsic hydrophobic nature and surface nanoroughness of the nanofiber morphology. Utilizing Zwitterionic/PVDF-HFP and Zwitterionic/PVDF-HFP/Ag webs led to hydrophobicity reduction. The static water contact angle test was performed with drops of nonionic water (5 μL) [4].

In the Fe_3O_4/PVDF nanofiber web, changing the nanoparticle concentration or electrospinning voltage changes the web hydrophobicity. For this purpose, Figure 10 shows a water contact angle test for rGO/TiO2/PVDF webs. At room temperature, the test was performed with a rame-hart DROPimage by dropping 2 μL of nonionic water onto webs. An average of 5 measurements and a 2-sample t-test were conducted. The results showed that the contact angle decreases by increasing the concentration of nanoparticles. A possible explanation is nanofiber surface morphology and diameter, which are essential to the web hydrophobicity. The web's average roughness increases by increasing nanoparticle concentration. Consequently, it reduced the surface tension and water contact angle [31]. Modifying these nanofibers with 1H,1H,2H, and 2H-perfluorodecalin trimethoxysilane could make more hydrophobic and even superhydrophobic webs. At -2 kV or 10 kV, the contact angle was 153° [32].

2.5. Mechanical properties

Although the PVDF webs have excellent mechanical properties, doping is helpful to improve them. GO and TiO2 are brittle materials, but PVDF is ductile. By doping, a mixture of both properties (more flexibility because of PVDF and more strength because of GO and TiO2) is obtained, but the percentages of each material should be optimized. Otherwise, the composite is nearly brittle or ductile. The stress-strain curves of the rGO/TiO_2/PVDF webs (Figure 11) showed linear elastic behavior (lower than 3 wt% nanoparticles) and then showed nonlinear behavior until failure. It is similar to nonwoven fabrics. The linear elastic step decreases by increasing nanoparticle concentration, and the nonlinear elastic step increased [31].

The stress-strain, force until failure, tension until failure, and yang modulus curves of TiO_2/PVDF webs are represented in Figure 12. The stress-strain curve showed linear elastic behavior under low strain and then showed nonlinear behavior (usually increasing trend) until it fails. This trend is similar to nonwoven fabrics. Force and tension increase until failure by rising in the nanofiber concentration despite the young modulus. This is due to filling the surface defects of the nanofiber with nanoparticles. However, after 3wt%, it reduces because the nanoparticles' adhesion on the nanofiber surface made it rigid. So, the best mechanical properties were for the 3wt% nanoparticles [2].

This section focuses on the applications of PVDF nanofibers, such as sensors, photocatalysts, and lithium-ion batteries, in which PVDF is used due to its excellent properties.

3. PVDF nanofibers applications

The PVDF has applications in many sensors owing to its piezo/pyro/ferroelectric properties. Some studies have been conducted on the subject. For instance, in pressure sensors, Ce3+/PVDF nanofibers were used. High pressure resulted in modification of spectral splitting, intensity, full width at half of maximum of the emission peak, and luminance lifetime. It is sufficient for applications, such as manometers that need pressure

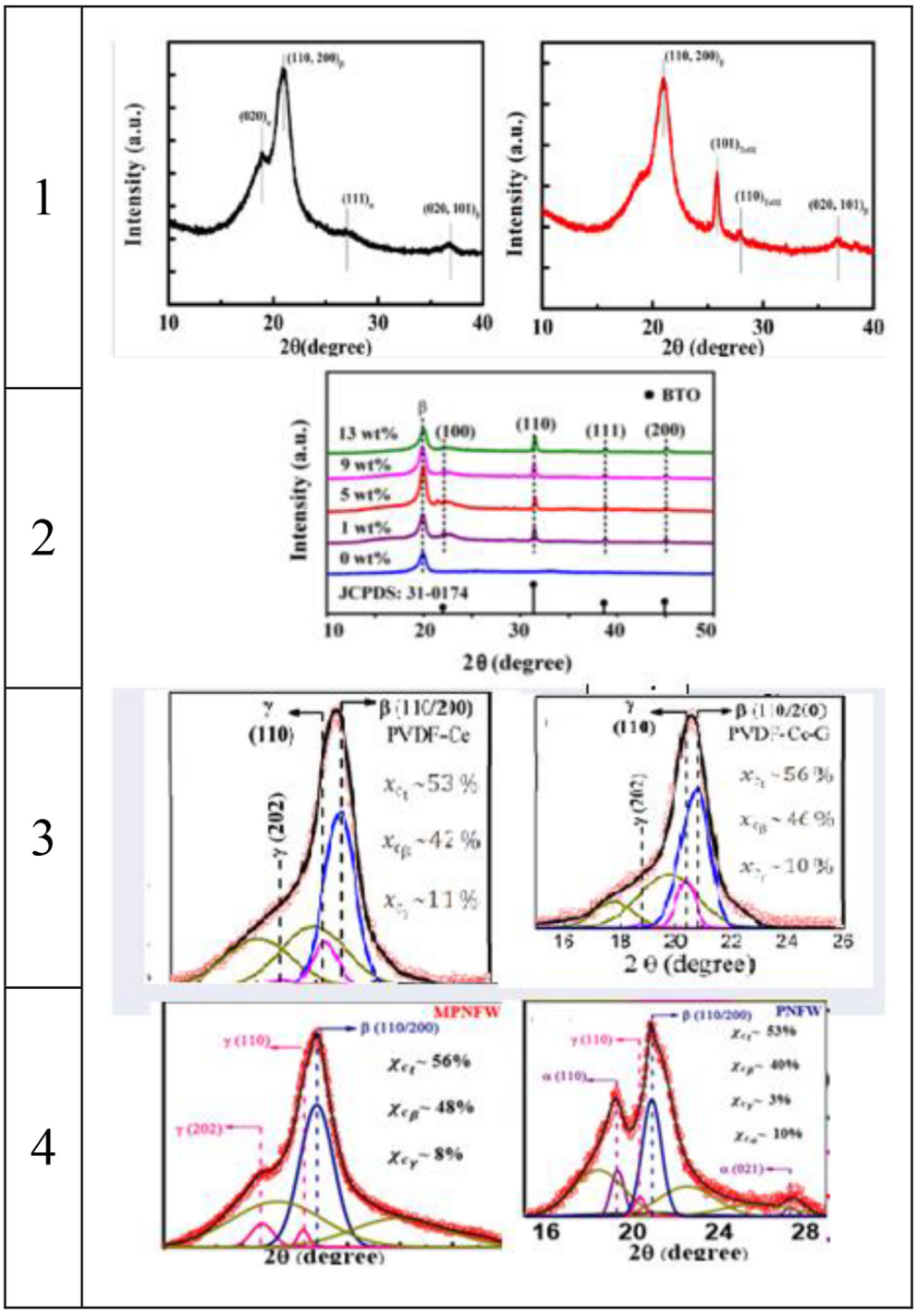

Figure 4. XRD images of nanofibers with/without dopants: 1) TiO_2 [9], 2) BTO [10], 3) G [11], and 4) MoS_2 [12].

calibration [5]. There are some examples of pressure sensors in Table 6. Also, a PVDF/AuNC hybrid device was used for recognizing the force and light simultaneously. This doping resulted in a higher β phase content and piezoelectric response. The presence of nanocages in nanofibers gave them the ability to convert the light into heat and then into electricity, resulting in a piezo/pyroelectric hybrid sensor [29].

In another study, the operation of the PVDF-HFP/(10–20 wt%) BTO electrospun nanofibers under an alternative pressure of 20 kPa considering electrical poling and nanoparticle concentration were investigated. In the 10–20 wt% region, the piezoelectric properties improved. Nevertheless, the nanoparticle clustering was reduced. At 20 wt%, the output voltage, current, and power were 9.63 V, 0.52 μA, and 7892.2 NW, respectively. After electrical polling, the output voltage, current, and power results were 11.7 V, 20.56 μA, and 1115.2 NW, respectively. These values, obtained after rectifying, are enough to light a small LED bulb [26].

Moreover, it has been shown that electrospun PVDF-HFP/NiFe2O4 (with 1, 2, and 3 wt%) nanofibers resulted in better alignment of dipoles and phase conversion. In 1 wt%, the web had a maximum dielectric constant of 118 in 1 Hz, which was 24 times higher than that of PVDF-HFP nanofibers. In 2 wt%, the output voltage was 4 V so that it can be applied in piezoelectric devices [23]. PVDF/nanoclay (15 wt%) nanofibers had a 90% electroactive phase and an output voltage and power density of 7 V and 68 μA/cm^2, respectively [33].

Table 4. Degrees of picks of different phases of PVDF [16].

PVDF	2θ(0)	Crystal plane
α	17.66	(100)
	18.30	(020)
	19.90	(110)
	26.56	(021)
β	20.26	(110) (200)
γ	18.5	(020)
	19.2	(002)
	20.04	(110)

In addition, composite nanofibers of PVDF/2wt% Ce–Fe_2O_3 and PVDF/2wt% Ce–Co_3O_4 were prepared. Incorporating magnetic nanoparticles had a substantial effect on the structural properties of the nanofibers, especially the β and γ phases of the polymer. In this regard, the interfacial properties were adjusted due to the increase in the electrostatic interaction of the filler-polymer. The outputs were 20 V (0.01 μA/cm^2) and 15 V under output voltage of 2.5. The nanoparticle size, filler-polymer interaction, and ion-dipole influenced the produced piezoelectric power [34].

The PVDF/$BiCl_3$ (2 wt%) nanofibers had an output voltage of 1.1 V, current of 2 μA, and surface power density of 0.2 μW/cm^2 (4.76 higher than PVDF) and could charge a capacitor by a bridge rectifier and lighten on a red LED [35]. Also, electrospun PVDF nanofibers, followed by hydrothermal production of ZnO (in the form of nanorods on the fiber), were achieved. The nanogenerator of the resulting web could convert sound (140 Hz, 116 dB) into electricity (1,12 V, 1.6 μA and 0.2 μW cm^{-2}) [36]. PVDF/AgNP (15 wt%) nanofibers could increase the electroactive phase and give a power of 7 × 10^{-4} W to convert sound to electricity [14]. The PVDF/ZnO nanofibers had an output voltage of 4.8 V under a wind force of 145 Pa [15].

A solution of DMF and THF with different ratios was used to prepare the PVDF/NP-ZnO nanofibers, and a lower concentration of ZnO and polymer and the same ratio gave the best fibers. By evaluating the effect

Table 5. Comparison of outputs of different studies for nanofibers with/without dopants.

Sample	Force (N)	Area (m^2)	Pressure (Pa)	Output voltage (V)	Sensitivity (V/KPa)	Current (nA)	Source
PVDF/no TiO_2	5	0.006	833.33	7	8.4	104	[9]
PVDF/no BTO	-	-	7000	-	-	4.8	[10]
PVDF/no G	8	825	6600	4.5	0.68	-	[11]
PVDF/no MoS_2	7	1257.142	8800	2.5	0.28	-	[12]
PVDF/TiO_2	5	0.006	833.33	11.5	13.8	176	[9]
PVDF/BTO	-	-	7000	-	-	12.5	[10]
PVDF/G	8	825	6600	11	1.66	-	[11]
PVDF/MoS_2	7	1257.142	8800	14	1.59	-	[12]

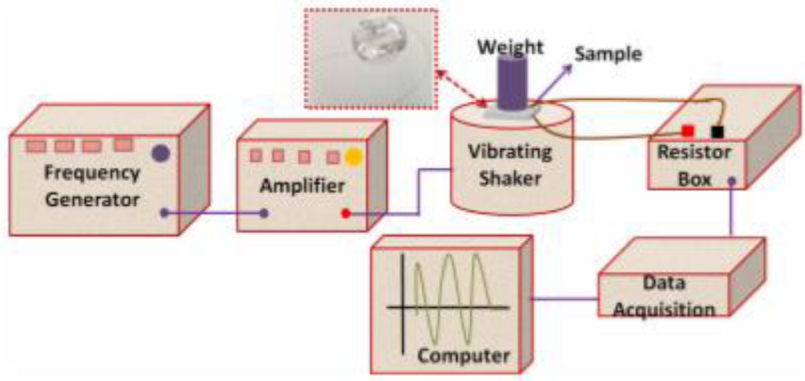

Figure 5. Schematic representation of the piezoelectric experimental setup [23].

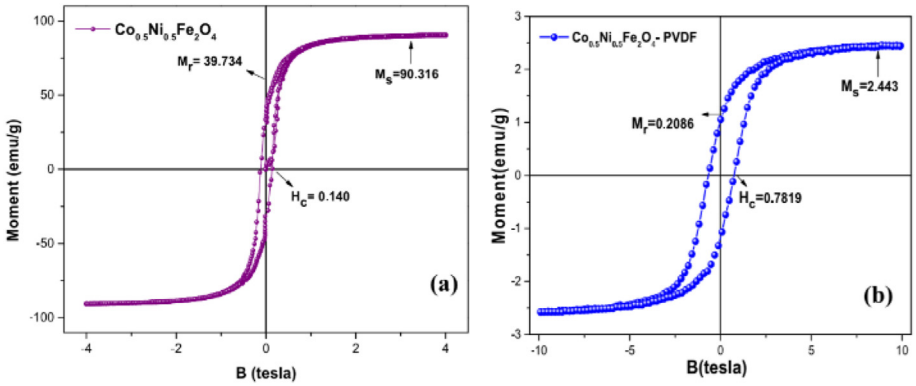

Figure 6. VSM plots of (a) Co0.5Ni0.5Fe2O4 pristine nanoparticles and (b) Co0.5Ni0.5Fe_2O_4-PVDF nanofiber membrane [25].

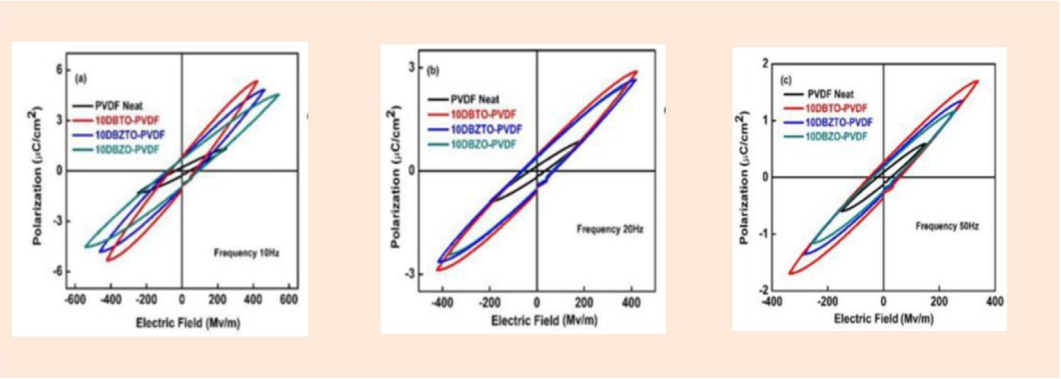

Figure 7. P–E loop of DBTO/DBZTO/DBZO-PVDF nanofibers at different frequencies (time): (a) 10 Hz, (b) 20 Hz, and (c) 50 Hz [28].

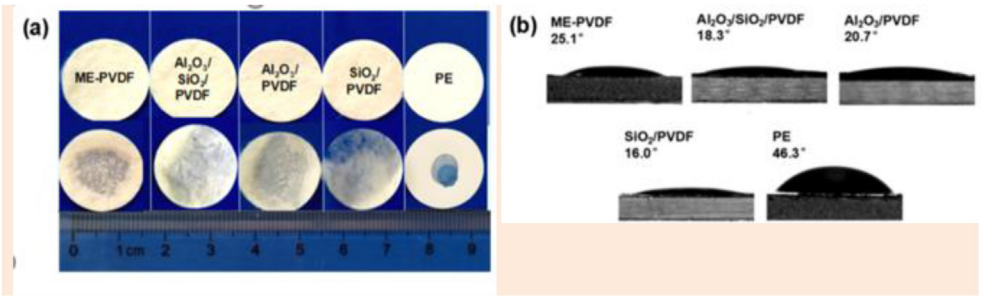

Figure 8. (a) photographs of the wetting behavior, and (b) initial contact angles of the ME-PVDF, Al_2O_3/SiO_2/PVDF, Al_2O_3/PVDF, SiO_2/PVDF, and PE membranes with the liquid electrolyte [8].

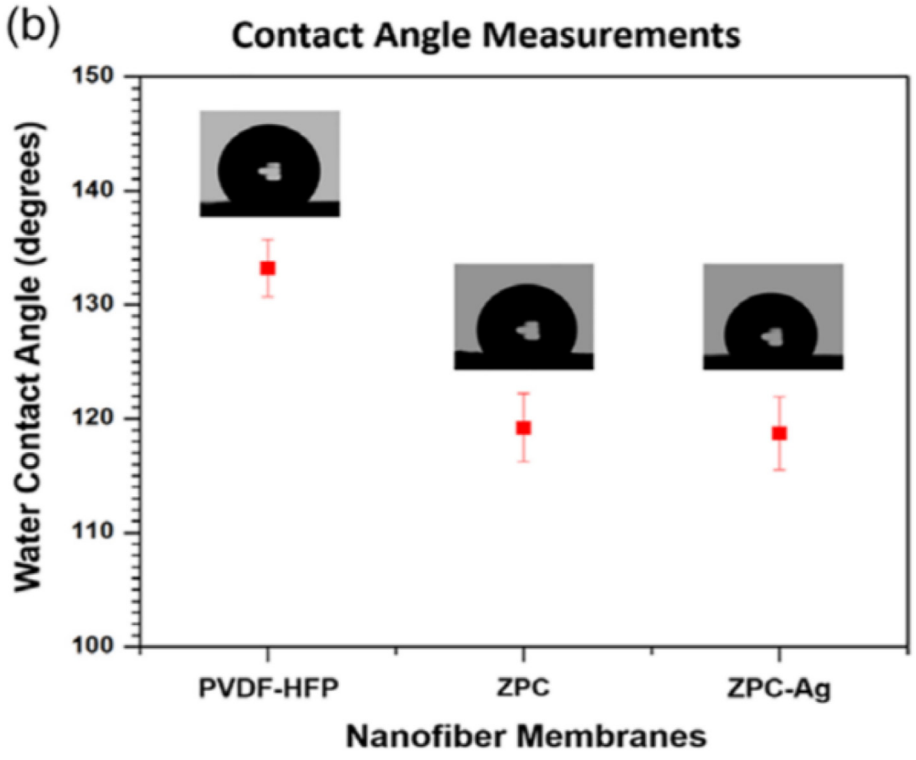

Figure 9. Static contact angle from water droplets (5 μL) on the PVDF-HFP, ZPC, and ZPC-Ag membranes [4]. Utilizing CNTs [6, 30] or plasma treatment [19] is a way to have (super)hydrophobic webs.

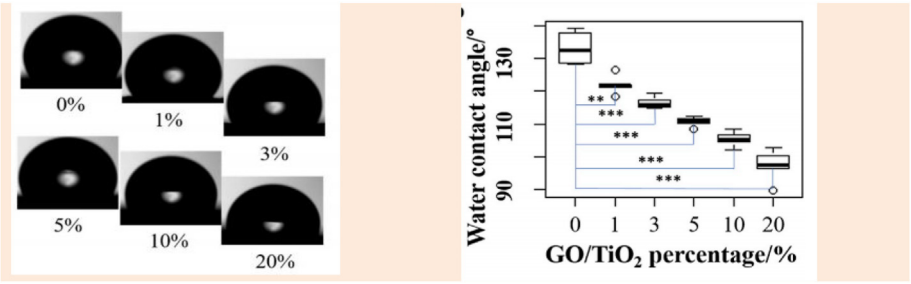

Figure 10. (a) water contact angles of the 0–20% samples (PVDF/GO/TiO2 nanofiber webs with rGO/TiO2 ratios of 0%, 1%, 3%, 5%, 10%, and 20%), and b) the water contact angle of samples and Welch two-sample t-test results (n – 5) [31].

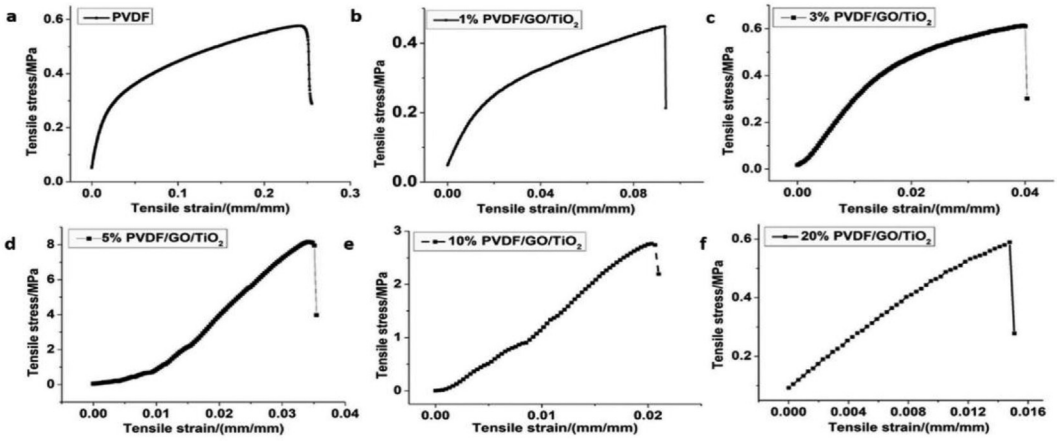

Figure 11. a–f) Tensile strain-stress curve of samples (PVDF/rGO/TiO_2 nanofiber webs) with varying rGO/TiO_2 concentrations [rGO/TiO_2 % = (rGO/TiO_2 amount/g)/(PVDF amount/g) × 100%] of 0%, 1%, 3%, 5%, 10%, and 20% [31].

of the process parameters, we found that the flow rate decreases at smaller distances to achieve more uniformity without beads or spraying. The maximum output power of the best sample was 32 nW/cm^2. More uniform and stretched fibers gave higher outputs of voltage and current [37]. The PVDF nanofibers can be used in tissue engineering and drug delivery. For example, PVDF nanofibers can be used in bone repair because of their flexibility and electrical microenvironment. It can be better when doped with other piezo materials, such as BTO [38]. Photoluminescence of rare-earth ion Eu^{3+} incorporated in polymers, such as PVDF and PEO can be used to produce electrospun nanofibers [3].

The PVDF/Eu^{3+} nanofibers have a good emission spectrum because of transferring $5D_0$ to $7F_2$, which is responsible for the luminance of Erium with a high-intensity ratio (2.61) (the ratio of the above transferring $5D_0$ to $7F_1$), which was higher than PEO/Eu^{3+} nanofibers. The reason is the excellent dispersion of erbium ions in PVDF chains, which increases their interaction. The population of ions in PVDF was more than in PEO. The application of these nanofibers is in photoluminescence fabrics and textiles. The presence of PMMA and PVDF in the Eu(TTA)3phen complex increased the sensitive fluorescent transfer intensity of $5D_0$ to $7F_2$ in the complex due to the effect of the polymer on coordination ions, which is the possibility of energy transfer of electrical dipoles, which resulted in a rise in luminance with a 612 nm peak [39].

On the other hand, metal catalyst materials with nanostructures and high specific surface areas are appropriate for methanol oxidation reactions as catalysts with applications in direct methanol fuel cells. Graphene is a 2D carbonic matter and the best material for platinum cells due to its excellent electrical conductivity, high specific surface area, and unique properties. Agglomeration of graphene can block the active sites of the catalyst. Thus, it reduces the catalytic activity. The production of 1D nanofibers has recently attracted the attention of researchers due to their lower affinity to agglomerate, high specific surface area, good thermal stability, and high porosity. Catalysts make more active catalytic sites in nanofibers and provide active morphological properties, resulting in active interactions with reactive molecules due to their small size and interconnected pores. A high specific surface area causes high dispersion of catalysts embedded in the polymer matrix [35].

The PVDF-Pt-Pd/RGO-CeO_2 composite nanofibers (decomposition at 490 °C) exhibited better thermal stability than PVDF nanofibers. A significant weight loss was observed for composite nanofibers (55.95 wt%) and PVDF nanofibers (51.6 wt%) in the temperature range of 460–500 °C. The residual amount of composite nanofibers was calculated to be 23.13 wt%, remarkably higher than that of PVDF nanofibers (0.042 wt%) due to the presence of PtePd and CeO_2 nanoparticles in the PVDF nanofibers [40].

Despite the advantages of PVDF and its derivatives for water purification, they suffer from bacterial migration due to their high porosity and surface roughness, resulting in the formation of constant layers. Agglomeration of bio layers includes bacteria and extracellular polymeric materials that make bio pollution, which is water-permeable and reduces the efficiency of water purification systems based on webs. Thus, many methods have been developed for engineering the resistance in front of bacteria pollution of fluoropolymer nanofibers for water purification. One way is applying antibacterial agents, such as silver nanoparticles in or on the nanofibers. These nanoparticles have good antibacterial activity against a wide range of bacteria related to silver ions that destroy the cell membrane of bacteria and overcome the membrane activity of enzymes. The discussion is on the strong keeping of silver nanoparticles in the nanofiber matrix by physical blending. It is due to the excitation of silver ions in the aqueous media of the nanofiber matrix. This antibacterial ability continues for 48 h [4].

An alternative method for the surface adhesion resistance of bacteria is the engineering of nanofiber surfaces by hydrophilic modifiers, such as

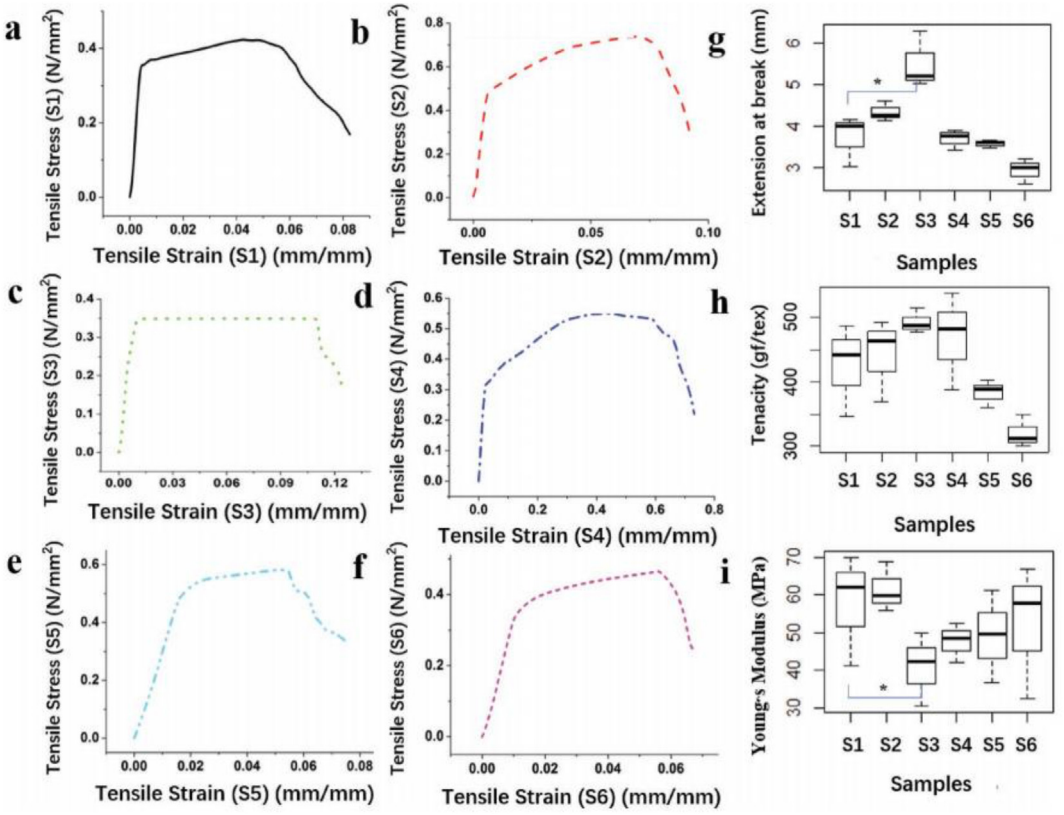

Figure 12. (a–f) Samples a-f show the tensile strain-stress curves of samples (PVDF/TiO_2 nanofiber webs) with varying TiO_2 concentrations of 0%, 1%, 3%, 5%, 10%, and 20%, respectively, g) average extension at the break for samples and Welch two-sample t-test results (n = 3), h) average load at the break for samples and Welch two-sample t-test results (n = 3), i) average Young's modulus of samples and Welch two-sample t-test results (n = 3). Note: "*" indicates $p < 0.05$, representing a significant difference at a 95% confidence level [2].

poly(ethylene glycol), poly(vinyl alcohol), and zwitterionic molecules. Among them, zwitterions have groups of phosphocreatine, sulfoβine, and carboxy βine, a promising group of materials to use in the new generation of bacteria anti-adhesions due to comparable operation of them with other works and, in some cases, better than hydrophilic modifiers. Their mechanism is unknown. Indeed, a neutral charge of zwitterion picks up more water molecules due to the high degree of hydrolysis of the surface that belongs to the reduction of bacterial adhesion. Among different zwitterionic monomers, sulfoβine methacrylate (SBMA) has advantages because of its ability to more polymerize and copolymerize than others. Various surface modifications, such as chemical, plasma, radiation, and flame retardants, exist for designing the surface of fluoropolymers with SBMA (resistat bacteria agents) [4].

Two kinds of nanofibers are used in a membrane to utilize both antibacterial and bacterial anti-adhesion to limit the bio pollution of the membrane. For stabilizing silver nanoparticles on PVDF-HFP nanofibers and blending SBMA molecules in polymeric structures for stable exposure to water, the electrospinning of two polymers was used to gather them randomly together. A non-volatile and environmentally safe organic compound was obtained by copolymerizing SBMA with methacryl polyhedral oligomeric silsesquioxane (MPOSS). The presence of PMMA improved the spinning ability and formation of even fibers. The results showed that the membrane under positive and negative warm bacterial strains for five days reduced the bacterial surface adhesion (90%), which was comparable with other membranes [4].

Combustion is a process that includes both fluid mechanics and chemical reactions simultaneously. The improvement of heat and the weight transfer rate of EMS received little attention recently. There was a metastable intermixed composite (MIC) based on Al by energetic metal-organic frameworks (EMOF) with a high specific surface area as reactive. The results showed that MIC significantly increased the released heat (3464 J/g). The combustion rate was more than five times faster than mechanical mixing, and efficiency improved. Additionally, the decomposition of EMOF could produce a large amount of gas on the surface layer that avoids cooking and pore formation. These pores are new channels for further chemical synthesis reactions and significantly improve the output energy [41].

Many anodic materials were prepared, in which their behavior in lithium-ion capacitors (LICs) is essential for reducing the unbalanced power capacity between electrodes owing to their effective role in the cyclic operation of LICs. The highly porous leaf-vein-like MnO_2@PVDF/TBAC nanofibers were made ready to improve the ion conductivity of the matrix and cyclic process. The Mno_2 nanofiber shell improved the cyclic process and avoided fast ion transfer between two electrodes. The nanofibers had excellent thermal stability (up to 170 °C), 73% porosity, and good ion conductivity (2.95 × 10-3 S/cm). The resulting LIC had a specific surface area of 19.5 F/g, a good rate, special cyclic stability (67.2% capacity after 1000 cycles remained), and high coulombic efficiency (near 100%) [42].

Rapid growth in the internet of things industry indicates the increasing need for humans. Among many technologies suggested for nonvisible communication, electronic textiles are considerable because of their benefits in human health control. Therefore, smart textronics help overcome rigid electronics. In this field, nanomaterials, such as nanoparticles, CNTs, and graphene are considerable due to their small sizes [6].

On the other hand, capacitive strain sensor fabric resulted from the dielectric fabric of PVDF-HFP and conductive PVDF-HFP/SWCNT fabric. The gauge factor, which was 130, had excellent mechanical properties. Moreover, the resulting morphology was appropriate for super-hydrophobic fabrics and better thermal and electrical conductivity, which are suitable for wearable heaters and heat waste screens [6].

Table 6. Various lanthanide-doped optical pressure sensors [5].

Material	Method Merits	Demerits		Optical pressure sensitivity
Ce^{3+} doped Fluorapatite	λ_{em}-Centroid shift and peak broadening	Very high-pressure sensitivity	Limited to 30 Gpa	0.67 nm/GPa
Eu^{3+} doped $aAlO_3$	Shift in charge transfer transition	High linearity, Simple approach of using variation in charge transfer state	Low-pressure sensitivity, Complexity due to Multiple peaks	14.4 cm^{-1}/kbar
Eu^{3+} doped Y_2O_{2S}	Shift in charge transfer transition	Simple	pressure in investigations extends only up to 24 GPS	-
$BaWO_4$: Ce single crystal	Host emission intensity	Singular emission peak	Not much change in spectral profile in terms of peak position and width, lower sensitivity	-
$KMgF_3$:Eu^{2+}	Change in Eu^{2+} spectral profile	Singular emission, Suitable for multi-cycle pressure experiments,	Low-pressure range up to 30 GPa, an issue with the toxic character of fluorine, issue in low temperature	-0.815 cm^{-1}/kbar
Nd^{3+}: Gd_3 $Sc_2Ga_3O_{12}$ crystal	Change in Nd^{3+} spectral profile	NIR P-T sensor in anvil cells at low temperatures and from ambient pressure up to 12 GPa	Several peaks, limited to the low-pressure zone	-8.8 cm^{-1}/GPS
$LaPO_4$/YPO: Yb^{3+} - Tm^{3+}	Change in the upconversion emission profile of Tm^{3+}	High-pressure sensitivity	Multiple peaks, complex phenomenon	-
SrB2O4:Sm^{2+} nanoparticles	Change in Sm2+ spectral profile	Sm^{2+}-based contactless pressure nano-sensor allows a very accurate pressure sensing (± 0.01 GPa)	Data available for Pup to 25 GPa only, lack of singular emission	0.24 nm/GPa
Cerium nitrate doped PVDF fiber	Change in Ce^{3+} spectral profile	Singular emission can work as low as well as high-pressure sensors, wide linear dynamic range	Moderate pressure sensitivity	0.28 nm/GPa
Ammonium Cerium sulfate doped PVDF fiber	Change in Ce^{3+} spectral profile	Singular emission can work as low as well as the high-pressure sensor	low-pressure sensitivity	0.10 nm/GPa

Table 7. Comparison of the reaction rate constants of some works [44].

Catalyst	Irradiation source	Degradation time (min)	The reaction rate constant (k, min^{-1})
MnOx@PVDF/MWCNTs	Sunlight	20	0.17
Mn_3O_4–MnO_2	Visible light	60	0.0456
HNTs/δ-MnO_2	Sunlight	60	0.05526
Mn_3O_4 nanoparticles	UV	25	0.0757
Codoped α-MnO_2 nanowires	Room light	30	0.122

Chargeable lithium-ion batteries have received increasing attention for electronic devices and electronic vehicles. In addition, increasing the energy density of lithium batteries is limited because of safety problems due to the formation of unusual lithium sediment during repetitive charge/discharge, leading to lithium dendrite formation with a combustion/explosion risk. The solid electrolytes are promising alternatives for liquid electrolytes due to their excellent mechanical properties (good under pressure, cleaning uneven lithium sediment, and delaying dendrite formation) and high electrochemical stability. In addition to nonorganic ceramic solid electrolytes, polymeric electrolytes are also interesting. Polymers, such as PVDF mix with lithium salts, but their low ion conductivity is a problem, so approaches, such as crosslinking, using two block copolymers, usual plasticizers, and adding ceramic fillers are given [43].

The PVDF-HFP/LiTFSI/LLZO electrolyte was prepared, and the presence of 10 wt% LIZO nanofibers helped improve the ion conductivity due to the design of continuous transfer paths for lithium ions. This electrolyte had excellent mechanical properties that resulted in stopping lithium dendrite growth. It had a good electrochemical range (5.2 V vs. Li/Li^+), profitable cyclic operation, and rate [43].

Designing separators resistant to high temperatures has an increased delivery ability, and high charge/discharge is necessary for high-performance lithium-ion batteries. The melt electrospun PVDF nanofibers were prepared by magnetic sputtering (Al_2O_3/SiO_2/PVDF, Al_2O_3/PVDF, and SiO2/PVDF). Among them, Al_2O_3/SiO_2/PVDF had excellent thermal stability (without shrinkage up to 130 °C and destroyed at 445 °C) and 340% electrolyte uptake. The presence of β phase and polar ceramic nanoparticles gave high conductivity eight times higher than commercial polyethylene. These webs had good discharge (161.5 mAh/g), rate after 100 cycles (84.3%), and capacitive in high intensity was 8C (49.8% better than commercial web) [9].

Photodegradation of rhodamine PVDF/TiO_2 (0–20 wt%) under visible light was investigated. Degradation of 20 wt% 80% in 6 h at 546 nm resulted. The color changed from red to orange, then to yellow, and finally to light yellow (complete degradation) by the degradation of pollutants. The reaction constant was calculated to estimate the degradation rate [2].

A tree-like web of helical-like PVDF/MWCNT nanofibers, followed by hydrothermal growth of MnO_x (these increased the specific surface areas), was used for dye degradation under natural sunlight radiation. This catalyst had excellent activity for various dyes under sunlight and even darkness [44]. Table 7 gives a comparison of the reaction rate constants of some works.

Materials with photothermal ability are fascinating due to using light energy. The (GO)/Bi_2S_3-PVDF/TPU nanofibers were prepared with (GO)/Bi_2S_3 as photothermal. The maximum light absorption of the web was approximately 90% at 400–2500 nm. In 300 s, the temperature change since the radiation was too fast and intense, and the equilibrium was 81°C [45].

In the PVDF/CNT membrane, the presence of interfacial polarization improved due to the piezoelectric CNTs. The high specific surface area made many sites for sound wave contact, which resulted in more sound absorption in the medium frequency region with a vibration/friction mechanism. Without CNTs, the absorption resulted in a low-frequency region. The results showed that acoustic foam with PVDF coverage is a good sound absorber from low to medium frequencies [46].

The electrospun PVDF tree-like nanofiber web was prepared. The results showed that this morphology reduced the pore size, narrowed the range of pore size distribution, and dramatically enhanced the specific surface area, so it had excellent filtration performance. The filtration efficiency with a basis weight of 1 g/m^2 to 0.26 μm NaCl particles was almost 100%, and the pressure drop was 124.2 Pa, comparable to ultra-low penetration air filters [47].

4. Conclusions

The PVDF-based nanofibers possess increased attention in research and application fields. This review summarizes and reviews the growth of this field because these materials are the main elements in developing many devices (sensors, fuel cells, photocatalysts, and piezoelectric devices) for future applications. Many research groups combine the PVDF nanofibers with other small molecules, polymers, and nanostructures. These systems have been developed for modern technology requirements and give new properties through many practical applications.

5. Outlook

As mentioned, the PVDF nanofibers have many applications, such as piezoelectric materials that are widely used in different applications. It is a polymer with many publications in nanogenerators. In comparison to triboelectric nanogenerators, they have lower outputs. So, the best way to increase outputs is using their composites. Recently, a polymer (PAN) has gotten much attention as a piezopolymer, and some authors have investigated PAN composite nanogenerators. However, the problem with this polymer is its price because it is more expensive than PVDF. Another difference is that making composites from PAN is harder than PVDF. Although PVDF composite nanofibers are getting lots of attention in filtration and bio applications, it raises the question that whether PAN takes the place of PVDF or not.

The paper has been pre-printed previously [48, 49].

Declarations

Author contribution statement

All authors listed have significantly contributed to the development and the writing of this article.

Funding statement

This research did not receive any specific grant from funding agencies in the public, commercial, or not-for-profit sectors.

Data availability statement

Data included in article/supp. material/referenced in article.

Declaration of interest's statement

The authors declare no conflict of interest.

Additional information

No additional information is available for this paper.

References

[1] A. Mahdavi Varposhti, et al., Enhancement of β-phase crystalline structure and piezoelectric properties of flexible PVDF/ionic liquid surfactant composite nanofibers for potential application in sensing and self-powering, Macromol. Mater. Eng. 305 (3) (2020), 1900796.
[2] L. Lou, et al., Visible light photocatalytic functional TiO2/PVDF nanofibers for dye pollutant degradation, Part. Part. Syst. Char. 36 (9) (2019), 1900091.
[3] S. Itankar, et al., Comparative photoluminescent study of PVDF/Eu3+ and PEO/Eu3 + electrospun nanofibers in photonic fabric, AIP Conference Proceedings (2019). AIP Publishing LLC.
[4] V. Anand Ganesh, et al., Engineering silver-zwitterionic composite nanofiber membrane for bacterial fouling resistance, J. Appl. Polym. Sci. 136 (22) (2019), 47580.
[5] C. Hernandez, et al., Performance evaluation of Ce3+ doped flexible PVDF fibers for efficient optical pressure sensors, Sensor Actuator Phys. 298 (2019), 111595.
[6] D.H. Ho, et al., Multifunctional smart textronics with blow-spun nonwoven fabrics, Adv. Funct. Mater. 29 (24) (2019), 1900025.
[7] J. Ning, et al., Tailoring the morphologies of PVDF nanofibers by interfacial diffusion during coaxial electrospinning, Mater. Des. 109 (2016) 264–269.
[8] S. Wu, et al., Ceramic nanoparticle-decorated melt-electrospun PVDF nanofiber membrane with enhanced performance as a Lithium-Ion Battery Separator, ACS Omega 4 (15) (2019) 16309–16317.
[9] M.M. Alam, et al., Biomechanical and acoustic energy harvesting from TiO2 nanoparticle modulated PVDF nanofiber made high-performance nanogenerator, ACS Appl. Energy Mater. 1 (7) (2018) 3103–3112.
[10] X. Hu, et al., Improved piezoelectric sensing performance of P (VDF–TrFE) nanofibers by utilizing BTO nanoparticles and penetrated electrodes, ACS Appl. Mater. Interfaces 11 (7) (2019) 7379–7386.
[11] S. Garain, et al., Design of in situ poled Ce3 +-doped electrospun PVDF/graphene composite nanofibers for fabrication of nanopressure sensor and ultrasensitive acoustic nanogenerator, ACS Appl. Mater. Interfaces 8 (7) (2016) 4532–4540.
[12] K. Maity, et al., Two-Dimensional piezoelectric MoS2-modulated nanogenerator and nano-sensor made of poly (vinylidene Fluoride) nanofiber webs for self-powered electronics and robotics, Energy Technol. 5 (2) (2017) 234–243.
[13] P. Sengupta, et al., A comparative assessment of poly (vinylidene fluoride)/conducting polymer electrospun nanofiber membranes for biomedical applications, J. Appl. Polym. Sci. 137 (37) (2020), 49115.
[14] C. Wu, M. Chou, Acoustic-electric conversion and piezoelectric properties of electrospun polyvinylidene fluoride/silver nanofibrous membranes, Express Polym. Lett. 14 (2) (2020).
[15] M.M. Alam, et al., An effective wind energy harvester of paper ash-mediated rapidly synthesized ZnO nanoparticle-interfaced electrospun PVDF fiber, ACS Sustain. Chem. Eng. 6 (1) (2018) 292–299.
[16] P. Martins, et al., Electroactive phases of poly (vinylidene fluoride): determination, processing and applications, Prog. Polym. Sci. 39 (4) (2014) 683–706.
[17] S.K. Ghosh, D. Mandal, Synergistically enhanced piezoelectric output in highly aligned 1D polymer nanofibers integrated all-fiber nanogenerator for wearable nano-tactile sensor, Nano Energy 53 (2018) 245–257.
[18] M.M. Abolhasani, et al., Thermodynamic approach to tailor porosity in piezoelectric polymer fibers for application in nanogenerators, Nano Energy 62 (2019) 594–600.
[19] C. Wan, C.R. Bowen, Multiscale-structuring of polyvinylidene fluoride for energy harvesting: the impact of molecular-, micro-and macro-structure, J. Mater. Chem. 5 (7) (2017) 3091–3128.
[20] C. Lang, et al., High-sensitivity acoustic sensors from nanofibre webs, Nat. Commun. 7 (1) (2016) 1–7.
[21] Z. Moarref, et al., Treatment of PVDF/ZnO Electrospun Fibrious Mat with Graphene Oxide Followed by Thermal Reduction to Produce Mechanical to Electrical Converter, Amirkabir University of Technology, 2017.
[22] S. Park, et al., Energy harvesting efficiency of piezoelectric polymer film with graphene and metal electrodes, Sci. Rep. 7 (1) (2017) 1–8.
[23] D. Ponnamma, et al., Electrospun nanofibers of PVDF-HFP composites containing magnetic nickel ferrite for energy harvesting application, Mater. Chem. Phys. 239 (2020), 122257.
[24] T. Zheng, et al., Local probing of magnetoelectric properties of PVDF/Fe3O4 electrospun nanofibers by piezoresponse force microscopy, Nanotechnology 28 (6) (2017), 065707.
[25] G.A. Kaur, et al., Modification of structural and magnetic properties of Co0. 5Ni0. 5Fe2O4 nanoparticles embedded Polyvinylidene Fluoride nanofiber membrane via electrospinning method, Nano-Struct. Nano-Objects 22 (2020), 100428.
[26] S.H. Lee, et al., Fabrication and characterization of piezoelectric composite nanofibers based on poly (vinylidene fluoride-co-hexafluoropropylene) and barium titanate nanoparticle, Fibers Polym. 21 (3) (2020) 473–479.
[27] M. Kushwah, et al., Dielectric, pyroelectric and polarization behavior of polyvinylidene fluoride (PVDF)-gold nanoparticles (AuNPs) nanocomposites, Vacuum 166 (2019) 298–306.
[28] A. Mayeen, et al., Flexible dopamine-functionalized BaTiO3/BaTiZrO3/BaZrO3-PVDF ferroelectric nanofibers for electrical energy storage, J. Alloys Compd. 837 (2020), 155492.
[29] H. Li, et al., Enhancing the tactile and near-infrared sensing capabilities of electrospun PVDF nanofibers with the use of gold nanocages, J. Mater. Chem. C 6 (38) (2018) 10263–10269.
[30] J. González-Benito, et al., PVDF based nanocomposites produced by solution blow spinning, structure and morphology induced by the presence of MWCNT and their consequences on some properties, Colloid Polym. Sci. 297 (7) (2019) 1105–1118.
[31] L. Lou, et al., Functional PVDF/rGO/TiO2 nanofiber webs for the removal of oil from water, Polymer 186 (2020), 122028.
[32] P. Jiang, et al., Research on hydrophobicity of electrospun Fe3O4/PVDF nanofiber membranes under different preparation conditions, Fullerenes, Nanotub. Carbon Nanostruct. 28 (5) (2020) 381–386.
[33] S. Tiwari, et al., Enhanced piezoelectric response in nanoclay induced electrospun PVDF nanofibers for energy harvesting, Energy 171 (2019) 485–492.
[34] H. Parangusan, et al., Toward high power generating piezoelectric nanofibers: influence of particle size and surface electrostatic interaction of Ce–Fe2O3 and Ce–Co3O4 on PVDF, ACS Omega 4 (4) (2019) 6312–6323.
[35] C. Chen, et al., Enhanced piezoelectric performance of BiCl3/PVDF nanofibers-based nanogenerators, Compos. Sci. Technol. 192 (2020), 108100.
[36] B. Sun, et al., Electrospun poly (vinylidene fluoride)-zinc oxide hierarchical composite fiber membrane as piezoelectric acoustoelectric nanogenerator, J. Mater. Sci. 54 (3) (2019) 2754–2762.
[37] S. Mansouri, et al., Investigation on the electrospun PVDF/NP-ZnO nanofibers for application in environmental energy harvesting, J. Mater. Res. Technol. 8 (2) (2019) 1608–1615.

[38] C. Shuai, et al., A strawberry-like Ag-decorated barium titanate enhances piezoelectric and antibacterial activities of polymer scaffold, Nano Energy 74 (2020), 104825.
[39] M. Dandekar, et al., Synthesis and photoluminescence study of electrospun nanofibers of Eu (TTA) 3Phen/PMMA-PVDF composite for photoluminescent fabric designing, AIP Conference Proceedings (2019). AIP Publishing LLC.
[40] M.F.R. Hanifah, et al., Electro-spun of novel PVDF-Pt-Pd/RGO-CeO2 composite nanofibers as the high potential of robust anode catalyst in direct methanol fuel cell: fabrication and characterization, Inorg. Chem. Commun. 107 (2019), 107487.
[41] W. He, et al., Energetic metastable n-Al@ PVDF/EMOF composite nanofibers with improved combustion performances, Chem. Eng. J. 383 (2020), 123146.
[42] X.-l. Shen, et al., A leaf-vein-like MnO2@ PVDF nanofiber gel polymer electrolyte matrix for Li-ion capacitor with excellent thermal stability and improved cyclability, Chem. Eng. J. 387 (2020), 124058.
[43] Y. Li, et al., Li7La3Zr2O12 ceramic nanofiber-incorporated composite polymer electrolytes for lithium metal batteries, J. Mater. Chem. 7 (7) (2019) 3391–3398.
[44] Z. Li, et al., Hierarchical MnOx@ PVDF/MWCNTs tree-like nanofiber membrane with high catalytic oxidation activity, J. Alloys Compd. 780 (2019) 805–815.
[45] W. Yang, et al., GO/Bi2S3 doped PVDF/TPU nanofiber membrane with enhanced photothermal performance, Int. J. Mol. Sci. 21 (12) (2020) 4224.
[46] C.M. Wu, M.H. Chou, Polymorphism, piezoelectricity and sound absorption of electrospun PVDF membranes with and without carbon nanotubes, Compos. Sci. Technol. 127 (2016) 127–133.
[47] Z. Li, et al., Fabrication of a polyvinylidene fluoride tree-like nanofiber web for ultra-high performance air filtration, RSC Adv. 6 (94) (2016) 91243–91249.
[48] S. Aghayari, Output Increasing Ways for Nanogenerators of PVDF Nanofibers: A Review, 2021.
[49] S. Aghayari, An Introduction to PVDF Nanofibers Properties, and Ways to Improve Them, and Reviewing Output Enhancing Methods for PVDF Nanofibers Nanogenerators, 2021.